(This is a sample cover image for this issue. The actual cover is not yet available at this time.)

Journal of Alloys and Compounds 555 (2013) 225–231

Contents lists available at SciVerse ScienceDirect

Journal of Alloys and Compounds

journal homepage: www.elsevier.com/locate/jalcom

Synthesis of nanosize and sintered $Mn_{0.3}Ni_{0.3}Zn_{0.4}Fe_2O_4$ ferrite and their structural and dielectric studies

U.B. Gawas [a], V.M.S. Verenkar [a,*], S.R. Barman [b], S.S. Meena [c], Pramod Bhatt [c]

[a] Department of Chemistry, Goa University, Taleigao Plateau, Goa 403206, India
[b] UGC-DAE Consortium for Scientific Research, Khandwa Road, Indore, 452001 Madhya Pradesh, India
[c] Solid State Physics Division, Bhabha Atomic Research Centre, Mumbai 400085, India

ARTICLE INFO

Article history:
Received 11 November 2012
Received in revised form 7 December 2012
Accepted 15 December 2012
Available online 22 December 2012

Keywords:
Nanoparticles
Mn–Ni–Zn ferrite
X-ray photoelectron spectroscopy
Mössbauer spectroscopy
Dielectric behaviour

ABSTRACT

$Mn_{0.3}Ni_{0.3}Zn_{0.4}Fe_2O_4$ ferrite nanoparticles were synthesized by thermally initiated autocatalytic decomposition of metal fumarato-hydrazinate complex. The chemical phase analysis has been carried out by X-ray powder diffraction method. The formation of complete ferrite phase occurred when the sample was annealed at 1100 °C. The physical properties such as lattice parameter, bulk density and porosity were studied. The infra red spectra displayed two bands characteristics of spinel ferrite due to M–O stretching vibrations in tetrahedral and octahedral sites. The X-ray photoelectron and Mössbauer spectroscopy were used to study the valence and distribution of cations in tetrahedral (A) and octahedral [B] sites of the spinel. The frequency dependence of the dielectric properties such as dielectric constant, ε', complex dielectric constant, ε'' and dielectric loss factor, tan δ, were studied at variable temperatures and reported in this paper.

1. Introduction

Ni–Zn ferrites are the technological materials having wide range of applications in electronic industries. These materials are particularly suitable for high frequency applications because of their high resistivity, low dielectric losses, mechanical strength, high curie temperatures and chemical stability. Hence, these materials find application in microwave devices, power transformer, rod antennas, read/write heads for high speed digital tapes etc. The only disadvantage of Ni–Zn ferrites is their low initial permeability at higher frequencies [1]. Mn–Zn ferrites, on the other hand, are widely used for magnetic application such as transformer cores, noise filters, recording heads due to their high permeability and saturation magnetization [2]. However, these ferrites also have certain limitations for magnetic applications at high frequencies, because of their low resistivity and hence high eddy current losses. For high frequency magnetic applications, ferrite should posses high permeability as well as high resistivity to reduce eddy current losses. Therefore, an appropriate combination of these two ferrites, can result in the material with enhanced properties, more suitable for high frequency application than Mn–Zn ferrites and Ni–Zn ferrites [3]. It is well established fact that, the magnetic and electrical properties of ferrites are sensitive to the cation distributions, which in turn depend on the method of synthesis. Hence, there is growing interest in the newer and newer synthetic strategies to prepare ferrites with best possible properties. Many authors have studied the magnetic, electric and dielectric characteristics of Mn–Ni–Zn ferrite system, prepared using various synthetic routes like conventional ceramic technique [4–6] and non-conventional techniques like sol–gel [7–9], co-precipitation [10], etc. Very few studies are reported on the detail structural characterization of Mn–Ni–Zn ferrite system. In this paper, we are reporting the synthesis, detailed structural characterization, X-ray photoelectron spectroscopy (XPS), Mössbauer studies and dielectric properties of $Mn_{0.3}Ni_{0.3}Zn_{0.4}Fe_2O_4$ ferrite nanoparticles (as synthesized) as well as one sintered at 1200 °C for 1 h in air.

2. Experimental

The polycrystalline nanoparticles of $Mn_{0.3}Ni_{0.3}Zn_{0.4}Fe_2O_4$ was synthesised by a non-conventional fumarato hydrazinate precursor method. The starting materials used were manganese chloride (99.0%, SD fine chemicals, India), zinc chloride (99.0%, SD fine chemicals, India), sodium fumarate (99.0%, SD fine chemicals, India), nickel chloride (99.0%, SD fine chemicals, India), hydrazine hydrate (99.0%, SD fine chemicals, India) and iron powder (99.9%, Merck, Germany). The detailed synthesis procedure of the precursor is reported elsewhere [11]. The yellow colour precursor complex was calcined at 400 °C for 5 h. The structure and phase purity of the ferrite was determined using X-ray diffractometer (Philips-PW 3710) with Cu K_α radiations and Ni filter. Transmission electron micrograph (TEM) of 'as synthesized' ferrite powder was recorded on electron microscope (JEOL-JEM 2100F). The scanning electron micrograph (SEM) of sintered pellet was recorded on (JEOL-JSM 5800LV). The infrared analysis of samples was carried out using infrared spectrophotometer (Shimadzu FTIR-IR prestige 21 series). The X-ray photoelectron spectroscopic (XPS) data of 'as synthesized' $Mn_{0.3}Ni_{0.3}Zn_{0.4}Fe_2O_4$ ferrite was recorded with the specimen

* Corresponding author. Tel.: +91 832 6519321; fax: +91 832 2452886.
E-mail address: vmsv@rediffmail.com (V.M.S. Verenkar).

0925-8388/$ - see front matter © 2012 Elsevier B.V. All rights reserved.
http://dx.doi.org/10.1016/j.jallcom.2012.12.054

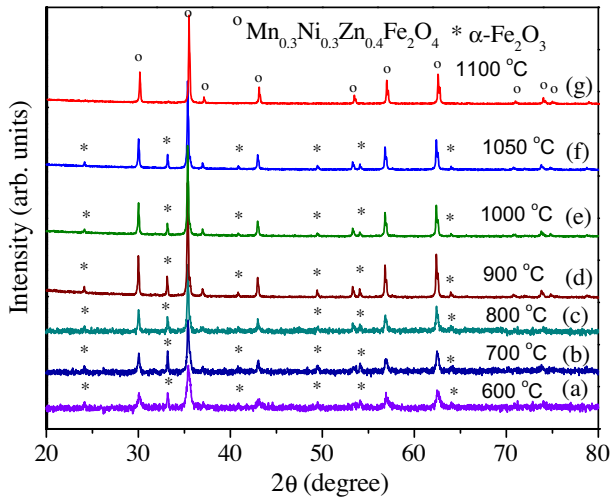

Fig. 1. XRD patterns of $Mn_{0.3}Ni_{0.3}Zn_{0.4}Fe_2O_4$ nanoparticles annealed at different temperatures (a) 600 °C/5 h, (b) 700 °C/5 h, (c) 800 °C/5 h, (d) 900 °C/5 h, (e) 1000 °C/5 h, (f) 1050/5 h, and (g) 1100 °C/1 h.

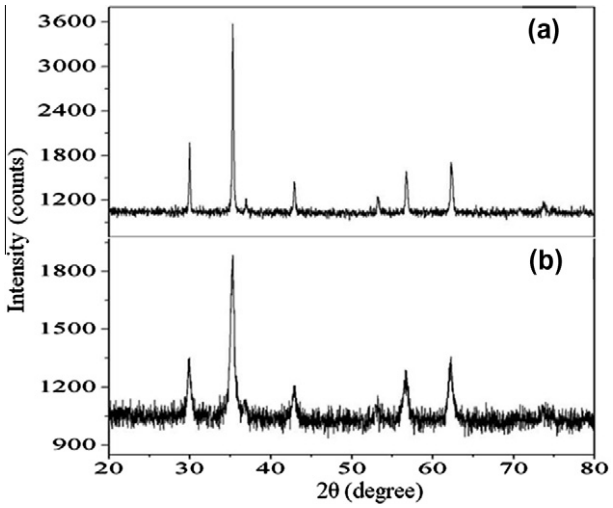

Fig. 2. XRD patterns of (a) as synthesized and (b) sintered $Mn_{0.3}Ni_{0.3}Zn_{0.4}Fe_2O_4$ samples.

mounted on a specially designed sample holder [12] at a base pressure of 3×10^{-10} mbar. An electron analyzer from SPECS Surface Nano Analysis GmbH, Germany and an Al-K_α laboratory X-ray source have been used for photoelectron spectroscopy measurements. The Mössbauer spectra of samples were recorded using a Mössbauer spectrometer (Nucleonix Systems Pvt. Ltd., Hyderabad, India) operated in constant acceleration mode (triangular wave) in transmission geometry at room temperature. The source employed was Co-57 in Rh matrix of strength 50 mCi. The calibration of the velocity scale was done by using an enriched α-^{57}Fe metal foil. The line width (inner) of calibration spectra was 0.26 mm/s. All Mössbauer spectra were fitted by using a Win-Normos fit program. The 'as synthesized' ferrite nanopowder was pelletized and preheated for 5 h at 800 °C. This preheated pellet was then ground for 2 h and pelletized again under pressure of 7 tons for 3 min (diameter 10 mm and thickness 2 mm), which was then sintered in air at 1200 °C for 1 h. The capacitance and dielectric measurements were carried out in the frequency range 20 Hz to 10 MHz using LCR metre (Wayne Kerr-6500P). The samples were pressed into circular disc shaped pellets, and silver coating was done on adjacent faces to make the parallel plate capacitor geometry with ferrite material as the dielectric medium.

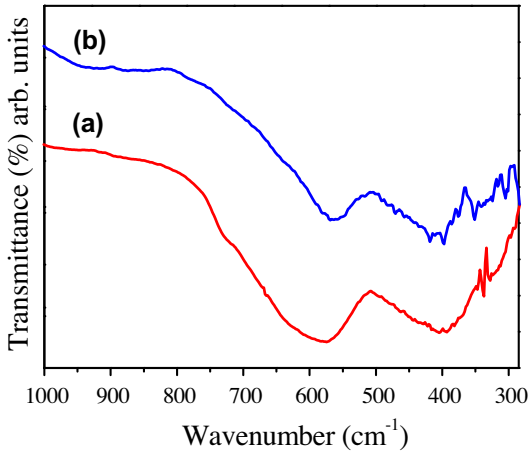

Fig. 3. IR spectra of (a) as synthesized and (b) sintered $Mn_{0.3}Ni_{0.3}Zn_{0.4}Fe_2O_4$ samples.

Table 2
Infrared absorption frequencies (cm^{-1}) of 'as synthesized' and sintered $Mn_{0.3}Ni_{0.3}Zn_{0.4}Fe_2O_4$ samples.

Sample	Tetra (γ_1)	Octahedral bands (γ_2 γ_3)			Lattice vibration (γ_4)		
As synthesized	577	394	338	329	276	254	224
Sintered	569	397	351	325	280	254	225

The dielectric constant (ε') of the ferrites sample was calculated by using the relation,

$$\varepsilon' = \frac{C_p \times t}{\varepsilon_0 A} \quad (1)$$

where ε' is the dielectric constant, ε_0 is free space permittivity (8.854×10^{-12} pF/cm), C_P is the capacitance of the sample in pF, t is the thickness of the specimen (cm) and A is area of cross section (cm^2).

The dielectric loss tangent ($\tan \delta$) was calculated by using the relation:

$$\tan \delta = \frac{1}{Q} \quad (2)$$

where Q is the quality factor.The complex dielectric constant (ε'') of the ferrite samples is given by:

$$\varepsilon'' = \varepsilon' \tan \delta \quad (3)$$

The dielectric constant (ε') and loss tangent ($\tan \delta$) was measured from room temperature to 275 °C.

3. Results and discussions

The X-ray diffraction (XRD) patterns of the samples annealed at different temperatures from 600 °C to 1100 °C are given in the Fig. 1. It was observed that, the ferrite samples decompose to Fe_2O_3 and Mn_2O_3, when annealing at 600 °C and above, in the air atmosphere. A prominent impurity peak, corresponding to α-Fe_2O_3, appears in the XRD patterns of samples annealed at or above 600 °C, whose intensity goes on increasing as the annealing temperature was increased up to 900 °C (Fig. 1a–d). However, when the same sample was heated (annealed) above 900 °C, the intensity of impurity peaks starts decreasing and completely disappears at 1100 °C (Fig. 1g) due to the dissolution of α-Fe_2O_3 and Mn_2O_3 to

Table 1
Lattice parameter (Å), X-ray density (g/cc), measured density (g/cc), porosity (%) and particle size (nm/μm), of the 'as synthesized' and sintered $Mn_{0.3}Ni_{0.3}Zn_{0.4}Fe_2O_4$ samples.

Sample	Lattice parameter	X-ray density	Measured density	Porosity	Particle size/grain size
As synthesized	8.4150	5.26	3.52	33.1	10–30 nm
Sintered	8.4177	5.25	4.87	7.23	2–4 μm

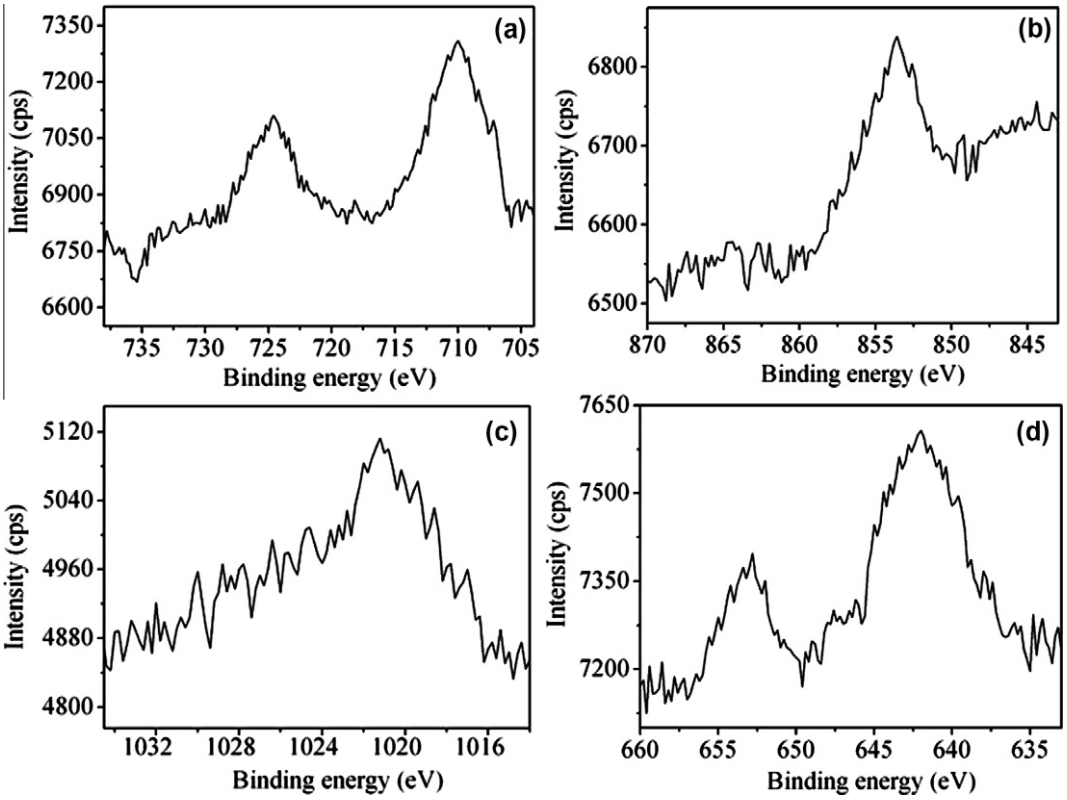

Fig. 4. Core level XPS spectra of the 'as synthesized' $Mn_{0.3}Ni_{0.3}Zn_{0.4}Fe_2O_4$ sample (a) Fe2p, (b) Ni2p, (c) Zn2p and (d) Mn2p.

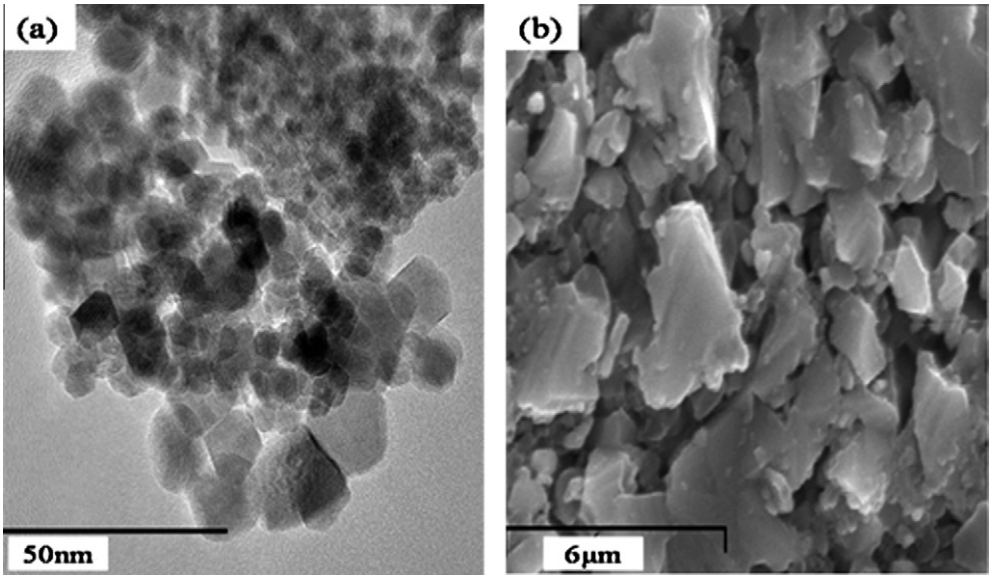

Fig. 5. TEM of (a) as synthesized and (b) SEM of sintered $Mn_{0.3}Ni_{0.3}Zn_{0.4}Fe_2O_4$ samples.

give single phase ferrite. The sample was further sintered at 1200 °C for 1 h. The XRD pattern of the sample sintered in air atmosphere at 1200 °C for 1 h (Fig. 2b), display all the peaks characteristics of cubic spinel structure which match with the similar results previously reported for the Mn–Zn ferrite system [13]. The XRD parameters such as lattice constant, X-ray density and porosity (Table 1) are in agreement with the reported values [14], while the measured density was found to be higher than that reported for ferrite, prepared by conventional method.

The normal and inverse cubic spinel ferrites shows four IR peaks, representing four fundamentals bands of ferrites [15,16]. It has been reported that, the first three fundamental bands are due to the M–O stretching vibrations in tetrahedral and octahedral site in cubic structure of ferrites, while the fourth one is because of lattice vibrations [17]. The Fig. 3(a) and (b) shows the IR spectra of both 'as synthesized' and sintered samples. The high frequency bands, ν_1 (569–577 cm^{-1}) and ν_2 (394–397 cm^{-1}) are attributed to Fe^{3+}–O^{2-} stretching vibrations in the tetrahedral and octahedral

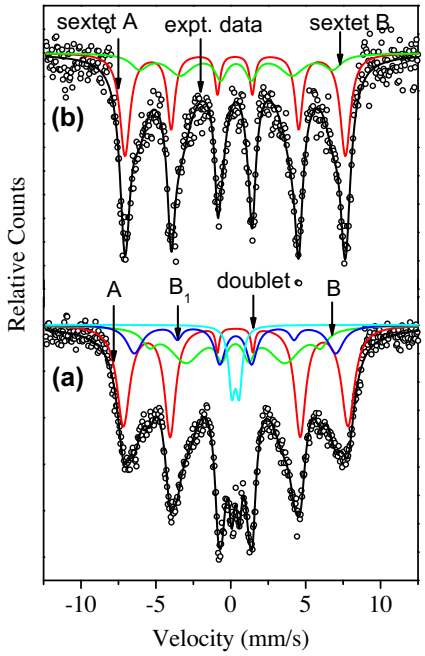

Fig. 6. Room temperature Mössbauer spectra of (a) as synthesized and (b) sintered $Mn_{0.3}Ni_{0.3}Zn_{0.4}Fe_2O_4$ samples.

sites, respectively. The third vibrational frequency bands, γ_3 (325–351 cm^{-1}) is associated with the divalent M^{2+}–O^{2-} stretching in octahedral site and the fourth vibrational bands, γ_4 between 225 and 280 cm^{-1} (not shown in the given figure) are attributed to the lattice vibrations [18]. It may be noted that, the absorption frequency of γ_1 band is decreased, while that of γ_2 is increased (Table 2) after sintering, which may be due to the transfer of larger Zn^{2+} and Mn^{2+} from octahedral to the tetrahedral site in the crystal structure of ferrite.

The Fig. 4(a)–(d) represents the XPS core level spectra of Fe2p, Mn2p, Ni2p and Zn2p of 'as synthesized' $Mn_{0.3}Ni_{0.3}Zn_{0.4}Fe_2O_4$ sample. The $Fe^{3+}2p_{3/2}$ peak is always associated with a satellite peak at 8.0 eV higher than the main peak, while $Fe^{2+}2p_{3/2}$ is associated with a satellite peak at 6.0 eV above the main peak. If, both Fe^{3+} and Fe^{2+} ion are present in the material then, it results in a broad background over the region ~710–720 eV, due to overlapping of satellite peaks of both ions. The 'as synthesized' $Mn_{0.3}Ni_{0.3}Zn_{0.4}Fe_2O_4$ ferrite powder sample shows a main peak at 711.2 eV due to $Fe^{3+}2p_{3/2}$ (Fig. 4a) and a satellite peak is observed at 719.2 eV, which indicates that, the surface of the ferrite contains iron in its trivalent state only [19]. In addition to this the binding energy of $Fe^{3+}2p_{1/2}$ was obtained in the present study at 724.6 eV. The $Ni^{2+}2p_{3/2}$ peak is observed at 854.8 eV (Fig. 4b), while the same peak in $NiFe_2O_4$ appears at 855.1 eV. The decrease in binding energy is reported in substituted ferrites, which is due to the distribution of Ni^{2+} in tetrahedral and octahedral sites in cubic structure of spinel ferrites. The Ni^{2+}2p3/2 peak in NiO is always associated with a satellite peak at 1–2 eV along the main peak. However, no such satellite peak is observed in the spectrum of the present sample under study for Ni^{2+}, hence it can be concluded that Ni^{2+} ions are present only in spinel structure [20]. The Zn^{2+}2p peak is observed at 1021.4 eV (Fig. 4c) in the XPS spectrum. The Zn^{2+} ions have preference for tetrahedral site in spinel structure in bulk material. While in the nanocrystalline materials, considerable concentration of Zn^{+2} ions occurs at octahedral sites, which results slightly higher binding energies for its 2p peak [21]. The IR and Mössbauer results in the present studies also support this observation. The $Mn2p_{3/2}$ and $Mn2p_{1/2}$ core-level peaks (Fig. 4d) centred at 642.8 eV and 653.9 eV results either from Mn^{2+} or Mn^{4+} since, the spectra of these ions overlap and it is very difficult to distinguish between these ions from their XPS spectra. However, since the valence of other cations present in the sample is not changed during the formation of ferrite, manganese should be present in divalent state [22,23]. The binding energy for O1s peak was observed at 529.9 eV, which is in agreement with the reported values for the O1s peak in the spinel lattice [24]. Hence, it can be concluded that the metal ions are present in their proper valence in the crystal structure of 'as synthesized' $Mn_{0.3}Ni_{0.3}Zn_{0.4}Fe_2O_4$ ferrite.

The Fig. 5(a) is the TEM of 'as synthesized' $Mn_{0.3}Ni_{0.3}Zn_{0.4}Fe_2O_4$ ferrite which shows grain size of 10–20 nm while Fig. 5(b) is the SEM of the same sample sintered at 1200 °C which shows average grain size of around 4 μm.

The Fig. 6(a) and (b) shows the Mössbauer spectra of 'as synthesized' and sintered $Mn_{0.3}Ni_{0.3}Zn_{0.4}Fe_2O_4$ ferrite, respectively. The Table 3 gives the magnetic hyperfine field values (H_{hf}), isomer shift (δ), quadrupole splitting (Δ), linewidth (Γ) and relative areas (R_A) in percentage of tetrahedral and octahedral sites of Fe ions. In the mixed $Mn_{0.3}Ni_{0.3}Zn_{0.4}Fe_2O_4$ ferrite, Zn ions have strong preference for the tetrahedral sites, while Ni ions have strong preference for the octahedral sites. Mn ions also occupy octahedral sites albeit with small preference. Mössbauer spectrum of as synthesized sample exhibits a superposition of three zeeman sextets due to ferromagnetic particles and a doublet due to superparamagnetic behaviour of nano-sized particles which is as per reported trends [25,26]. In general, a system of magnetic nanoparticles becomes single-domain below a critical size. In the single-domain state, these nanoparticales become superparamagnetic with a blocking temperature (T_B). Below T_B, the magnetization of such superparamagnetic nanoparticles fluctuates spontaneously with a relaxation time (τ) $\leqslant 10^{-9}$ s. As a result, in the Mössbuer spectrum, magnetic splitting disappears resulting in a superparamagnetic doublet, as observed in Fig. 6(a) and also reported in the literature [26,27]. The relative percentage of sextet to doublet patterns is found to be 97.2:2.8 indicating that the superparamagnetic fraction is small.

The Mössbauer spectrum of sintered sample exhibits a superposition of two Zeeman sextets. The assignment of sextets corresponding to A- and B-sites in sintered sample was done on the basis of isomer shift. The isomer shift of tetrahedral site was found

Table 3
Room temperature Mössbauer effect parameters; isomer shift (δ), quadrupole splitting (Δ), hyperfine field (H_{hf}), inner line width (Γ), relative area (R_A) of 'as synthesized' and sintered $Mn_{0.3}Ni_{0.3}Zn_{0.4}Fe_2O_4$ samples.

Sample	Site	δ (mm/s)[a]	Δ (mm/s)	H_{hf} (Tesla)	R_A (%)	Γ (mm/s)
As synthesized	Sextet 1, (A)	0.319	0.035	46.2	29.4	0.278
	Sextet 2, [B]	0.313	−0.01	36.3	58.3	1.034
	Sextet 3, [B_1]	0.316	0.021	41.5	9.5	0.485
	Doublet	0.307	0.480	–	2.8	0.53
Sintered	Sextet 1, (A)	0.287	0.016	45.62	44.75	0.427
	Sextet 2, [B]	0.353	0.005	40.02	55.25	0.937

[a] Isomer shift values are relative to α-Fe metal foil (δ = 0.0 mm/s), (): tetrahedral, []: octahedral.

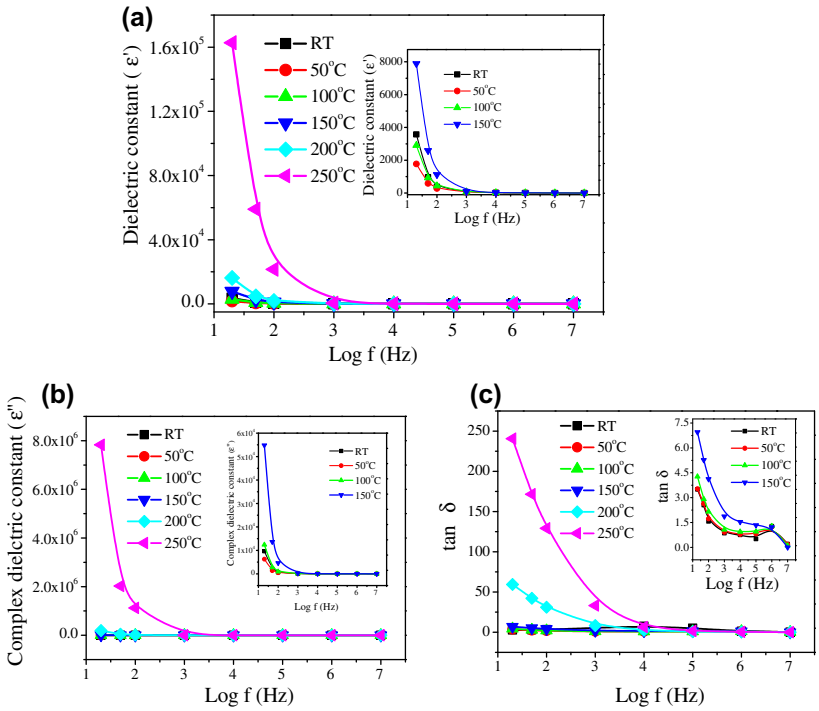

Fig. 7. Variation of (a) real, (b) imaginary part of dielectric constant and (c) loss tangent at different temperatures for 'as synthesized' $Mn_{0.3}Ni_{0.3}Zn_{0.4}Fe_2O_4$ sample as a function of frequency.

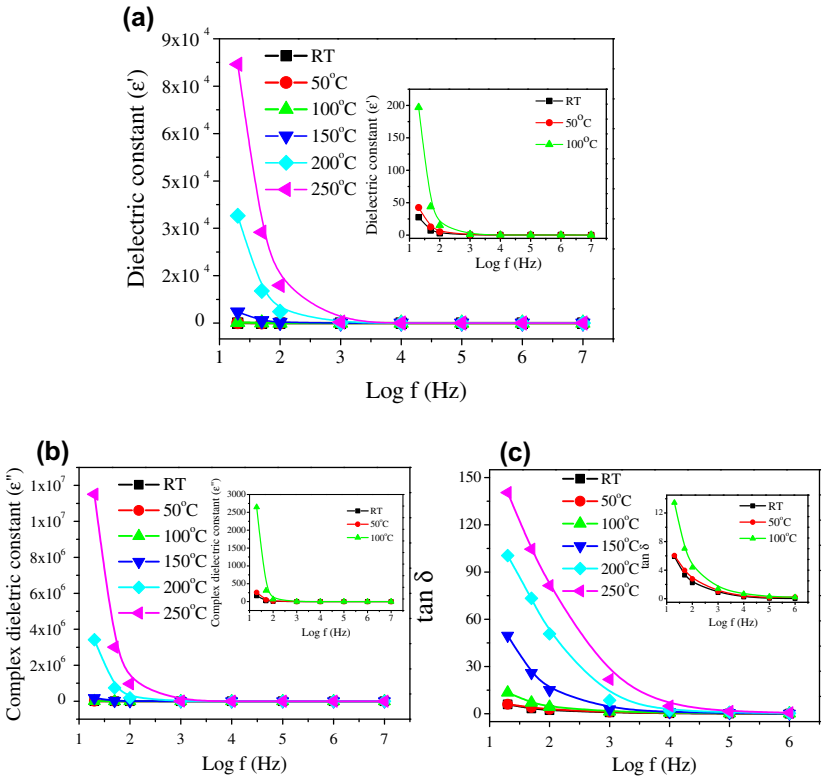

Fig. 8. Variation of (a) real, (b) imaginary part of dielectric constant and (c) loss tangent at different temperatures for sintered $Mn_{0.3}Ni_{0.3}Zn_{0.4}Fe_2O_4$ sample as a function of frequency.

to be lower than that of octahedral site (Table 3) which was observed by others [26]. The Fe^{3+} ion in tetrahedral site has more s-electron density than that in octahedral site. It results in shorter Fe-O distance in tetrahedral site than that in octahedral site [28]. So, the sextet with a lower isomer shift corresponds to the A-site, and the sextet having a higher isomer shift represents the B-site.

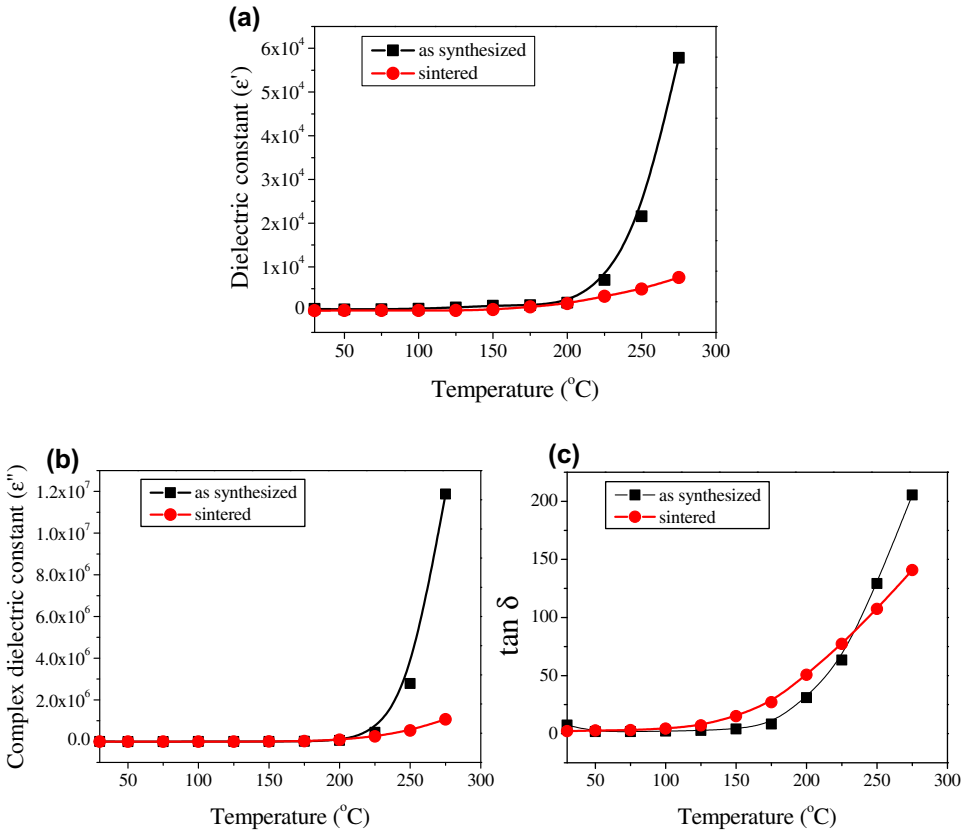

Fig. 9. Variation of (a) real part of dielectric constant, (b) imaginary part of dielectric constant and (c) loss tangent at 100 Hz frequency for 'as synthesized' and sintered $Mn_{0.3}Ni_{0.3}Zn_{0.4}Fe_2O_4$ samples as a function of temperature.

Areas in relative percentage in tetrahedral and octahedral sites are 55.3% and 44.7%, respectively in sintered sample.

The isomer shift (δ) values for 'as synthesized' are nearly same for all three sextets, so assignment of sextets has been done on the basis of magnetic hyperfine field (H_{hf}). In the sintered sample, the H_{hf} value for tetrahedral site was higher than that of octahedral site, so the sextet with higher H_{hf} is belongs to the tetrahedral site. Isomer shift (δ) values for 'as synthesized' and sintered samples are 0.287–0.319 mms^{-1} for tetrahedral site and 0.313–0.353 mms^{-1} for octahedral site, respectively with respect to α-Fe (δ = 0.00 mms^{-1}). This indicates that, Fe was in Fe^{3+} high spin ionic state. The observed values of isomer shift are comparatively less than the expected value of 0.8 mm/s for the Fe^{2+} ion, which indicates that the formation of Fe^{2+} ion does not occur during sintering [29–31]. Thus, the sample maintains its stoichiometry even after sintering in air atmosphere. Except for doublet (Δ = 0.48 and R_A = 2.8%) in 'as synthesized' sample, the quadrupole splitting (Δ) values for 'as synthesized' and sintered samples are nearly 0.0 mm/s, suggesting that Fe^{3+} ions show cubic symmetry of polyhedron. The comparatively higher value of Δ for doublet is attributed to an increase in the asymmetry around the iron ions.

The frequency variation (20 Hz to 10 MHz) of real and imaginary part of the dielectric constant of both 'as synthesized' and sintered $Mn_{0.3}Ni_{0.3}Zn_{0.4}Fe_2O_4$ ferrite was studied from room temperature to 275 °C (Fig. 7a, b and Fig. 8a, b). It was observed that, the dielectric constant shows rapid decrease up to 1 kHz, followed by a slow decrease from 1 kHz to 10 kHz, and was nearly independent of frequency from 10 kHz to 10 MHz. The very high values of dielectric constant (10^3–10^5) were observed for 'as synthesized' nanocrystalline $Mn_{0.3}Ni_{0.3}Zn_{0.4}Fe_2O_4$ ferrite (Fig. 7a) may be due of its ultrafine size. Since in an ultrafine state both, the number of grains and grain boundaries are large as compared to the bulk state resulting into more complex phenomena. Also the surface area of individual nanosize grains is large; hence the possibility of surface polarisation is also large. In a lower frequency region, surface polarisation contributes predominantly than electronic or ionic polarisation in determining the dielectric properties of ferrite materials [32]. The decrease in dielectric constant with increasing frequency is a normal behaviour observed in most of the ferromagnetic materials. The low value of dielectric constant observed in the present study for sintered sample than those reported using conventional methods, was due to the low concentration of Fe^{2+} ions in the sample and lower loss of Zn^{2+} ions during sintering. Zinc evaporation is pronounced only when the ferrite are sintered above 1200 °C. The SEM micrograph of sintered sample (Fig. 5b) consists of relatively small grains (4 μm). It can be seen from the micrograph that, the grain size and size spread are much smaller. The small grains are preferred in ferrites as oxidation advances faster, leading to oxidation of Fe^{2+} ions to Fe^{3+}, resulting in the lower values of dielectric constants. The Figs. 7c and 8c shows the variation of dielectric loss as a function of frequency (20 Hz–10 MHz) of 'as synthesized' and sintered ferrites, respectively, at different temperatures. The dielectric dispersion exhibited by the sample is very small, extends up to 10^3 Hz and is insignificant at higher frequencies. The dielectric loss gives the loss of energy from the applied field into the sample. This is caused by domain wall resonance. At higher frequencies, the losses are found to be low, since domain wall motion is inhibited and magnetization is forced to change rotation. The dielectric dispersion curve can be explained on the basis of Koop's theory [33], based on the Maxwell–Wagner model for the inhomogeneous double structure [34]. In ferrites, it is well known that the samples consist of well-conducting grains separated by poorly conducting grain boundaries [33]. The electrons reach the grain boundary through hopping

and if the grain boundary resistance is high enough, the electrons pile up at the grain boundaries and produce polarisation. However, as the frequency of the applied field is increased, the electrons reverse their direction of motion more often. This decreases the probability of electrons reaching the grain boundary and as a result the polarisation decreases. Therefore, the dielectric constant decreases with increasing frequency of the applied field. The dielectric constant value increases with temperature at all frequencies (Fig. 9a and b). The increase in the value of the dielectric constant with an increase in temperature was very large at lower frequency of ~1 kHz, while at higher frequencies ~1 MHz, the increase was very small. At low frequencies, the dipolar and interfacial polarizations are known to play the dominant role. Both these polarizations are strongly temperature dependent. The interfacial polarisation increases with temperature due to creation of crystal defects while dipolar polarisation decreases with increase in temperature. The rapid increase in the dielectric constant with increase in temperature at low frequencies suggests that the effect of temperature is more pronounced on the interfacial polarisation than on the dipolar polarisation [35]. At high frequencies, electronic and ionic polarizations are the main contributor and their temperature dependence is insignificant. Hence, it results in constant value of dielectric at high frequency. A dielectric loss (Fig. 9c) shows gradual increase with increasing temperature up to 150 °C while rapid increase in dielectric loss is observed above 150 °C.

4. Conclusion

Nanosize $Mn_{0.3}Ni_{0.3}Zn_{0.4}Fe_2O_4$ ferrite synthesized by thermally initiated autocatalytic decomposition of metal fumarato-hydrazinate complex. Formation of single phase $Mn_{0.3}Ni_{0.3}Zn_{0.4}Fe_2O_4$ occurs at 1100 °C when sintered in air atmosphere. Transfer of divalent Mn^{2+} and Zn^{2+} ions was observed from octahedral [B] to tetrahedral (A) sites after sintering as indicated by IR and Mössbauer spectra. XPS studies indicate the proper valence of the metal ions in the 'as synthesized' $Mn_{0.3}Ni_{0.3}Zn_{0.4}Fe_2O_4$ ferrite. The Mössbauer spectral studies has shown the high spin ionic state of Fe^{3+} in both 'as synthesized' and sintered $Mn_{0.3}Ni_{0.3}Zn_{0.4}Fe_2O_4$ ferrite and quadrupole splitting value suggests the cubic symmetry of polyhedron. The isomer shift values also confirm that there is no formation of Fe^{2+} ions during sintering. The dielectric constant and dielectric loss is found to be higher for 'as synthesized' sample due to its nanosize nature while the sintered sample shows relatively very low values of dielectric constant and dielectric loss. This ferrite under study can be a promising candidate for high frequency applications.

Acknowledgements

Authors are grateful for the financial support from DST, New Delhi through the Nano Mission project, No. SR/NM/NS-86/2009 and also under FIST. The authors are also thankful to UGC, New Delhi for the financial support under SAP and minor project. The authors would like to acknowledge SAIF-IIT Bombay and Mr. Girish Prabhu, N.I.O., Goa for recording TEM micrograph and XRD of the samples, respectively. We thank Mr. Abhishek Rai for photoemission measurements.

References

[1] A. Goldman, Modern Technology, second ed., John Wiley, New York, 1990. p. 71.
[2] A.K. Singh, T.C. Goel, R.G. Mendiratta, J. Magn. Magn. Mater. 57 (2003) 1040.
[3] A.K. Singh, T.C. Goel, R.G. Mendiratta, J. Magn. Magn. Mater. 281 (2004) 276.
[4] B.V. Bhise, M.B. Dongare, S.A. Patil, S.R. Sawant, J. Mater. Sci. Lett. 10 (1991) 922.
[5] H. Zhong, H. Zhang, J. Magn. Magn. Mater. 283 (2004) 247.
[6] K. Sun, Z. Lan, Z. Yu, L. Li, H. Ji, Z. Xu, Mater. Chem. Phys. 113 (2009) 797.
[7] A.R. Bueno, M.L. Gregori, M.C.S. Nobrega, Mater. Chem. Phys. 105 (2007) 229.
[8] S.E. Shirsath, B.G. Toksha, R.H. Kadam, S.M. Patange, D.R. Mane, G.S. Jangam, A. Ghasemi, J. Phys. Chem. Solids 71 (2010) 1669.
[9] A.K. Singh, T.C. Goel, R.G. Mendirattaa, J. Appl. Phys. 92 (71) (2002) 3872.
[10] C. Venkataraju, G. Sathishkumar, K. Sivakumar, J. Magn. Magn. Mater. 322 (2010) 230.
[11] U.B. Gawas, S.C. Mojumdar, V.M.S. Verenkar, J. Therm. Anal. Calorim. 96 (1) (2009) 49.
[12] R.S. Dhaka, A.K. Shukla, M. Maniraj, S.W. D'Souza, J. Nayak, S.R. Barman, Rev. Sci. Instrum. 81 (2010) 43907.
[13] P. Hua, H. Yang, D. Pan, H. Wang, J. Tian, S. Zhang, X. Wang, A.A. Volinsky, J. Magn. Magn. Mater. 322 (2010) 173.
[14] A.A. Sattar, H.M. El-Sayed, K.M. El-Shokrofy, M.M. El-Tabey, J. Mater. Sci. 42 (2007) 149.
[15] D. Ravinder, Mater. Lett. 40 (1999) 205.
[16] R.D. Waldron, Phys. Rev. 99 (1955) 1727.
[17] K. Mohan, Y.C. Venudhar, J. Mater. Sci. Lett. 18 (1999) 13.
[18] A.A. Sattar, H.M. El-Sayed, K.M. El-Shokrofy, M.M. El-Tabey, J. Appl. Sci. 5 (1) (2005) 162.
[19] T.J. Daou, G. Pourroy, S. Begin-Colin, J.M. Greneche, C. Ulhaq-Bouillet, P. Legare, P. Bernhardt, C. Leuvrey, G. Rogez, Chem. Mater. 18 (2006) 4399.
[20] V.K. Mittal, P. Chandramohan, S. Bera, M.P. Srinivasan, S. Velmurugan, S.V. Narasimhan, Solid State Commun. 137 (2006) 6.
[21] P. Gao, E.V. Rebrov, T.M.W.G.M. Verhoeven, J.C. Schouten, R. Kleismit, G. Kozlowski, J. Cetnar, Z. Turgut, G. Subramanyam, J. Appl. Phys. 107 (2010) 044317-1.
[22] G. Bonsdorfa, K. Schaferb, K. Teskea, H. Langbeina, H. Ullmanna, Solid State Ionics 110 (1998) 73.
[23] J. Hu, M.C.L. Irene, G.H. Chen, Langmuir 21 (2005) 11173.
[24] V.K. Mittal, S. Bera, R. Nithya, M.P. Srinivasan, S. Velmurugan, S.V. Narasimhan, J. Nucl. Mater. 335 (2004) 302.
[25] S. Yan, W. Ling, E. Zhou, J. Cryst. Growth 273 (2004) 226.
[26] K. Mandal, S. Pan Mandal, P. Agudo, M. Pal, Appl. Surf. Sci. 182 (2001) 386.
[27] R. Ghosh, L. Pradhan, Y.P. Devi, S.S. Meena, R. Tewari, A. Kumar, S. Sharma, N.S. Gajbhiye, R.K. Vatsa, B.N. Pandey, R.S. Ningthoujam, J. Mater. Chem. 21 (2011) 13388.
[28] S.S. Shinde, S.S. Meena, S.M. Yusuf, K.Y. Rajpure, J. Phys. Chem. C115 (2011) 3731.
[29] K. Sharma, S.S. Meena, S. Saxena, S.M. Yusuf, A. Srinivasan, G.P. Kothiyal, Mater. Chem. Phys. 133 (2012) 144.
[30] K. Sharma, S.S. Meena, C.L. Prajapat, S. Bhattacharya, Jagannath, M.R. Singh, S.M. Yusuf, G.P. Kothiyal, J. Magn. Magn. Mater. 321 (2009) 3821.
[31] K. Sharma, A. Dixit, S. Singh, Jagannath, S. Bhattacharya, C.L. Prajapat, P.K. Sharma, S.M. Yusuf, A.K. Tyagi, G.P. Kothiyal, Mater. Sci. Eng. C29 (2009) 2226.
[32] J.C. Maxwell, Electric and Magnetism, Oxford University Press, New York, 1973. p. 828.
[33] C.G. Koops, Phys. Rev. 83 (1951) 121.
[34] K.W. Wagner, Ann. Phys. 40 (1913) 817.
[35] K. Iwachi, Y. Ikeda, Phys. Status Solidi A 93 (1986) 309.